ELSEVIER

NeuroImage

www.elsevier.com/locate/ynimg
NeuroImage 34 (2007) 1588–1599

# Age-related water diffusion changes in human brain: A voxel-based approach

Estela Càmara,[a,b,*] Nils Bodammer,[c] Antoni Rodríguez-Fornells,[a,d] and Claus Tempelmann[c]

[a]*Faculty of Psychology, University of Barcelona, Passeig de la Vall d'Hebrón 171, 08035, Barcelona, Spain*
[b]*Department of Neuropsychology, Otto von Guericke University, Magdeburg, Germany*
[c]*Klinik für Neurologie II, Otto von Guericke University, Magdeburg, Germany*
[d]*Institució Catalana de Recerca i Estudis Avançats (ICREA), Barcelona, Spain*

Received 12 May 2006; revised 20 September 2006; accepted 22 September 2006
Available online 22 December 2006

**The aim of the present study is to investigate age-related changes in water self-diffusion in cerebral white matter by analysing diffusion-weighted MRI from a sample of 54 healthy volunteers. A voxel-based analysis of the relative anisotropy and the apparent diffusion coefficients was performed by applying an optimized normalization protocol. Linear regression analysis revealed significant correlations with age in the corpus callosum, prefrontal regions, the internal capsule, the hippocampal complex, and the putamen. However, in other regions, such as those surrounding the ventricles, the insula, or the inferior frontal plane, significant correlations between age and ADC were observed, presumably as a result of morphological age-related variations. A mask procedure was carried out in order to distinguish between morphological involvement and real age-related white matter changes.**

**Our results indicate that in interpreting the changes in each significant region it is necessary to proceed with precaution because the voxel-based statistical analysis might yield a mixture of two effects: (i) morphological changes that remain after the normalization procedure and (ii) actual diffusivity parameter changes. Anatomically defined regions of interest may help us to minimize morphologic involvement and draw comparisons with findings previously published.**


## Introduction

Normal brain development is a complex and dynamic process exhibiting a high degree of variability across the lifespan. Existing age-related magnetic resonance imaging (MRI) volumetric studies have revealed an increase in sulcal volume and an enlargement of the lateral ventricles, accompanied by a shrinkage in brain tissue volume (Good et al., 2001) occurring predominantly in the prefrontal and parietal lobes (Resnick et al., 2003). However, these studies have focused mainly on macrostructural changes and, consequently, they are limited in resolution. In contrast, neuropathological studies have reported age-related deterioration in the microstructure of white matter, including demyelination or axonal loss in the cerebral cortex (Marner et al., 2003).

Diffusion tensor imaging (DTI) has proved itself to be a suitable method for monitoring microstructural changes, neural architecture (Beaulieu, 2002) and possibly plasticity-related processes (Tovar-Moll et al., 2006). As such it is a promising tool for the quantitative estimation of brain organization and brain development (Moseley, 2002).

At the microscopic level, brain parenchymal structures have distinct boundaries, including axon membranes and myelin sheaths, which constrain the diffusional propagation of water molecules and force the latter in certain preferential directions. Thus, the water diffusion averaged over the individual voxels, as expressed by the apparent diffusion coefficient (ADC), is reduced in accordance with the local occurrence of these membranes. According to the present anisotropy of cellular structure, this reduction in diffusion due to membrane hindrance is also angular-dependent (Beaulieu, 2002). The degree of diffusion anisotropy can be specified using one of the anisotropy indices, e.g. the relative anisotropy index (RA) (Pierpaoli and Basser, 1996), which is calculated from the directionally dependent signal decay due to diffusion. As the diffusion properties ADC and RA are directly related to the microstructure of the medium studied, they can be used to characterize tissue and to detect possible histological changes due to physiological and pathological states. Both ADC and RA measures have been shown to reliably detect local white matter changes in normal aging (Nusbaum et al., 2001). Thus, the number of applications that DTI can offer in the study of aging and neurodegenerative disorders (Kubicki et al., 2002) has soared over the past several years. Most of the DTI aging studies have focused on region-of-interest (ROI) (Gideon et al., 1994; Abe et al., 2002; Sullivan and Pfefferbaum, 2003) or histogram analysis (Chen et al., 2001; Chun et al., 2000; Pfefferbaum and Sullivan, 2003). However, these methods only permit the description of diffusion properties at the regional or global level, respectively, i.e., beyond the method-inherent averaging of microstructural information over each voxel. Using ROI-based analysis, the spatial resolution

* Corresponding author. Fax: +34 934021363.
*E-mail address:* ecamara@ub.edu (E. Càmara).
**Available online on ScienceDirect (www.sciencedirect.com).**

1053-8119/$ - see front matter © 2006 Elsevier Inc. All rights reserved.
doi:10.1016/j.neuroimage.2006.09.045

provided by DTI is not exploited. In particular, region-of-interest analysis has several limitations, as for example, it is restricted to just the few regions chosen for analysis by a priori hypotheses. In this sense, the results obtained might be affected by the criteria chosen to define the ROIs because possible bias might be introduced due to manual or semi-automated definitions of the ROIs (Virta et al., 1999). The additional averaging over to some extent arbitrarily outlined regions also reduces spatial resolution. Therefore, ROI analysis might not be sensitive enough to detect some biologically meaningful differences which could be otherwise detected at the voxel level (Virta et al., 1999). Finally, subvolumes of the ROI might be inherently influenced by partial volume effects associated with tissue loss, gliosis or by compaction. These morphological changes might influence the detection of white matter differences after averaging. Given these concerns, the benefits of voxel-based analysis become apparent as an attractive method to investigate local age-related white matter changes in the whole brain. Voxel-based analysis has previously been applied to DTI data in aging studies in a preliminary study using a small sample of healthy volunteers (Nusbaum et al., 2001) and in a study comparing young and old age groups (Head et al., 2004). Recently, it has been used as an exploratory tool for the whole brain by Salat et al. (2005).

The main challenge facing voxel-based diffusion parameter analysis involves meeting the requirement for an optimal matching of the brains being compared. Thus, high demands are placed on the normalization procedure. By contrast, in the methodology related to voxel-based morphometry the objective is different, since in this case a slightly imperfect normalization is not only tolerable, it is even desired in order to keep anatomical differences on a mesoscopic scale (Ashburner and Friston, 2001). Standard normalization procedures, as provided, for example, by SPM, lead to a sufficient match between different brains at a macroscopic scale and remove global differences in anatomy. However, if the intention is to examine tissue properties at a voxel level, identical brain coordinates have to be compared across the whole study population, discarding even mesoscopic structural differences.

Unfortunately, this goal is almost impossible to achieve. First, brain structures, in particular the sulcal–gyral pattern, show considerable diversity across different brains, which makes the finding of a perfect match even by non-linear 3-D transformations unfeasible. Furthermore, a high degree of exactness of the normalization procedure requires high-dimensional parameter spaces in which the brain warps can be expanded and optimized. Thus, more degrees of freedom incur more potential local minima, leading to possibly erroneous results in the registration of the brain images (Ashburner et al., 2001). However, in the case of a moderate number of warping parameters, even large-scale anatomical differences, such as different ventricular volumes, might not be fully compensated by normalization. Additionally, neighbouring tissue might be forced to follow highly contrasted edges due to the application of non-perfectly adjusted brain warps. Consequently, the named sources of anatomical mismatch might have a considerable impact on inter-subject comparisons. Hence, analyses using voxel-size resolution require optimized normalization protocols, including the creation of a suitable internal-study brain template (Good et al., 2001), in order to minimize inter-subject anatomical variations as well as possible. A standard normalization procedure might not solve potential problems owing to the systematic effects caused by brain atrophy, which correlates with age (Good et al., 2001). In this sense, Salat et al. (2005) considered their voxel-based diffusion anisotropy maps of the whole brain as only exploratory measures, compared to ROI analysis. However, it is our belief that these maps do constitute a good starting point for a detailed analysis as long as additional checks are applied. The aim of the present study is to examine possible age-related white matter changes in healthy subjects based on ADC and RA whole brain data. For this purpose, a voxel-based linear regression analysis was performed using an optimized normalization protocol in order to facilitate the characterization of microstructural differences at a voxel level. However, special care needs to be taken when interpreting the results obtained with ADC data, which might potentially be affected at the tissue/CSF interfaces, because in these regions morphological changes related to age seem to be relatively large and the normalization procedure might not properly match the brain structures. In the case of RA images, considerable morphology-related effects might be derived from potential displacements of fibres that are not properly fitted by the normalization procedure. In this vein, comparisons with age-related MR volumetric studies (Good et al., 2001) can be helpful in order to roughly identify regions prone to morphological changes with age.

Therefore, it is essential to control any potential problems arising from the normalization procedure, especially in a study involving a large age range, where these systematic differences in brain structure may generate significant effects. For this reason, the combination of ROI analysis, which is not subject to normalization constraints, and voxel-based analysis could play an important role in validating the data. Therefore, additional ROI analysis was performed in three anatomically defined brain structures (genu and splenium of the corpus callosum and the putamen) in order to confirm our voxel-based findings at the regional level and to compare them with ROI analysis results published elsewhere.

An alternative method for detecting possible influences of non-perfect normalization in cross-sectional studies involves the introduction of tools designed to detect these artefacts. Here, we propose a mask procedure applicable to ADC images in order to distinguish morphologic involvement from real white matter changes.

## Methods

### *Subjects*

Fifty-four healthy volunteers underwent DTI brain examinations, 22 women and 32 men (mean age 37.3 ± 17.0, range 19–71 years). None of the participants reported to have a history of psychiatric or neurologic disorders. Written informed consent according to the approval of the Local Ethical Committee was obtained from all participants before MR examinations.

### *MRI acquisition protocol*

DTI was performed on a GE Signa Horizon LX 1.5 T neuro-optimized MR tomograph (General Electric Medical Systems, Milwaukee, WI, USA) employing a diffusion tensor spin echo EPI sequence. Diffusion weighting was conducted using the standard PGSE method. Images were measured using 3 mm thick slices, no gap, TR = 10 s, TE = 70 ms, 128 × 128 acquisition matrix, interpolated by zeropadding to 256 × 256, FOV 28 cm, 39 axial slices. Four averages were acquired per slice and diffusion gradient direction.

In order to obtain diffusion tensors, diffusion was measured along 12 non-collinear directions, chosen according to the DTI acquisition scheme proposed by Papadakis et al. (1999), and the values specified by Skare et al. (2000) using a single *b*-value of 1000 s/mm$^2$. For each gradient direction, inverted diffusion gradient polarity was measured as well, again collecting four averages each. Hence, a total of 24 diffusion-weighted measurements were performed. They were divided into four blocks, each one preceded by a non-diffusion-weighted acquisition.

*Image processing*

*Analysis of diffusion-weighted data*

First, the diffusion-weighted images were corrected for eddy-current-induced distortions, taking advantage of the symmetrical deformations caused by opposite diffusion gradient directions (Bodammer et al., 2004). Secondly, head motion correction was performed based on the non-diffusion-weighted images. The first non-diffusion-weighted image of each block was realigned with the first-likewise non-diffusion-weighted-image of the first series using the realignment algorithm provided by the Automated Image Registration (AIR) package (Woods et al., 1998). Then the determined transformation parameters were applied to the remaining diffusion-weighted images of the respective block.

In order to extract diffusion tensor elements from an over-determined set of diffusion-weighted images, singular value decomposition was used. Diffusion tensors were diagonalized extracting the eigenvectors and eigenvalues. Based on the eigenvalues, the ADC and RA diffusion parameters were calculated on a voxel-by-voxel basis.

*Optimized normalization protocol*

Normalization of all ADC and RA data sets to the same anatomical space was performed also based on the non-diffusion-weighted image volumes using a three-step processing scheme (Fig. 1). These image processing steps were carried out with SPM2 (Wellcome Department of Cognitive Neurology, Institute of Neurology, UK). Special effort was made to create an optimized study brain template offering study-inherent contrast and distortions, according to the applied sequence parameters and additionally including the averaged anatomical characteristics of all study participants. The detailed steps of the normalization procedure were as follows:

(1) First, the non-diffusion-weighted images ($b \approx 0$ s/mm$^2$) were normalized using the EPI-derived MNI template (ICBM 152, Montreal Neurological Institute) provided by SPM. After an initial affine transformation, an iterative non-linear normalization was applied using a lower threshold of 25 mm for the spatial periods of the discrete cosine basis functions by which brain warps are expanded in SPM (Ashburner and Friston, 1999). From the resulting normalized data sets a first preliminary study template was created by averaging.
(2) In a second run, the non-diffusion-weighted image volumes of all subjects were normalized again—but now using the study template that was created before in step (1). A second and final study template, which defines the anatomical space of the present study, was generated by averaging these newly normalized images after the extraction of only brain parenchyma. The extraction of brain tissue was performed by a three-class brain segmentation, i.e., segmentation of grey matter (GM), white matter (WM), and CSF/non-brain-tissue, retaining only voxels where the probability of belonging to GM or WM as assessed by SPM2 exceeded 0.8. The threshold was selected based on preliminary tests which showed that a lower threshold resulted less effective in removing non-brain voxels, whereas a higher threshold did not retain all brain parenchyma voxels.
(3) In a third step, based on the optimized protocol first introduced by Good et al. (2001), individual native-space brain parenchyma maps were extracted from the measured non-diffusion-weighted images and normalized to the final extracted-brain template. Parameters of the previous non-linear transformation were reapplied to the ADC and RA maps without Jacobian modulation of the signal intensities, generating the unmasked ADC and RA maps. Afterwards, normalized non-diffusion-weighted images were segmented. By merging of the GM and WM segments normalized binary brain mask images were created and applied to the ADC and RA maps. That is, a second set of masked ADC and RA images was obtained where only brain parenchyma was included. Moreover, a standard deviation (S.D.) map was computed from the binary mask images of the study participants.

In sum, two versions of the normalized ADC and RA maps were created, in order to be further used in statistical analysis: (i) one version in which they are reduced to the brain-parenchymal volume (masked) and (ii) the original parameter maps containing also non-brain tissue and CSF (unmasked). Finally, all individually normalized ADC and RA data sets were smoothed by convolving them with isotropic 8 mm and 4 mm FWHM (full width at half maximum) Gaussian kernels. We report only the 4 mm FWHM Gaussian kernel result because it preserved the same regional patterns as shown with the 8 mm kernel size, but with better spatial resolution.

*Voxel-based analysis*

Linear regression analysis was carried out for both sets of images (masked and non-masked images) using SPM99. Voxel-wise *t*-tests were performed to detect voxels where the slope of ADC or RA data against age as fitted by linear regression was significantly different from zero.

In order to estimate the extent of the interfacial areas between CSF and brain parenchyma, the voxel-wise standard deviations of all participants' binary mask images were calculated. The resulting standard deviation image varied between zero (the respective voxel corresponded to the same category for all subjects, i.e., either brain or non-brain) and 0.5 (for 50% of subjects the voxel corresponded to brain tissue, for another 50% to CSF or non-brain tissue). Thus, the standard deviation image presented its highest values in those voxels for which the probability over all the examined subjects to constitute the CSF/brain border was relatively high. Consequently, the standard deviation image allowed us to map potential CSF/parenchyma interfaces. Hence, we were able to use these maps to identify regions with noticeable normalization mismatch.

On the other hand, such brain boundary regions, where the normalization results were not optimal, should show considerable differences in the ADC-versus-age linear regression results dependent on whether binary brain masks were applied or not. This is due to the diffusion in CSF regions being reflected by high ADC

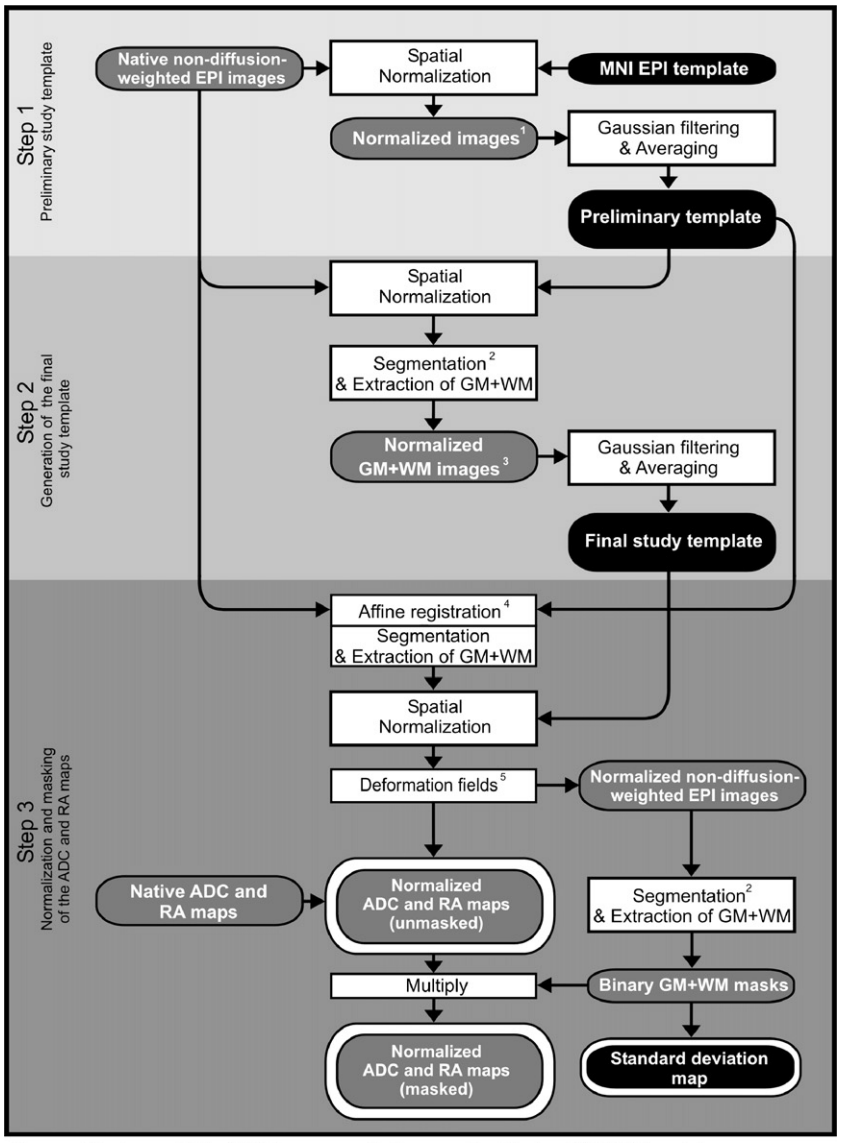


Fig. 1. Flowchart describing the three-step normalization procedure used in this study. In steps 1 and 2 the study template is optimized. In step 3 the normalization itself is performed, normalization transforms are applied to the ADC and RA maps, and a map showing the S.D. of the normalized binary brain mask images over all study participants is calculated. ADC, RA maps and the S.D. map are highlighted by white margins as these are the images which are further processed in statistical analysis or used as an indication for non-perfect normalization, respectively. Black-filled round-edged boxes represent images which only comprise one volume for the whole study, whereas grey boxes indicate series of individual image sets.

values, when no masking is applied, whereas the application of binary masks converts these values to zero. Therefore, ADC correlation maps should be inverted in regions close to CSF/parenchyma borders if the correlations do not reflect real white matter changes but rather inaccurate normalization. This interrelation was used to estimate whether significant regression results might have been caused by morphological or microstructural causes.

For the labelling of the white matter fibre tracts the DTI brain atlas by Wakana et al. (2004) was used.

*Region-of-interest analysis*

Four regions-of-interest (ROI), namely the genu and splenium of the corpus callosum and both putamina, were marked out in each participant's brain using the semi-automated procedure provided by MRIcro (Rorden C; University of South Carolina, Columbia, USA; http://www.sph.sc.edu/comd/rorden/mricro.html). These particular regions were chosen for this type of analysis because of their important role in diffusion tensor imaging and aging studies (Moseley et al., 2002; Head et al., 2004) (notably for

the corpus callosum), their high statistical effect size as observed in the voxel-based analysis (in the putamen), and their vicinity to the ventricles, which means they are especially prone to imperfect correction in the normalization process.

The outlines of these regions were identified in the RA maps, where they are easily isolated and differentiated. In order to minimize possible partial volume effects arising at the borders of the selected brain substructures the outermost layer of each marked region was reduced.

In the case of the corpus callosum, the segmentation of the genu and splenium ROIs was performed on non-normalized sagittally resliced RA images from 1 cm left to 1 cm right of the midsagittal plane. The genu was defined as the anterior 25% of the corpus callosum, while the splenium was the posterior 25%. Mean ADC and RA values were determined for each participant separately.

The putamen ROIs were seen on 4–5 axial slices. They were delimited by the surrounding internal and external capsule fibre tracts on the RA images in native space. The globus pallidus was excluded as much as possible, selecting only the less intensive voxels that presented a putamen shape.

Mean ROI ADC and RA values were extracted and correlated with age. Additionally, for the putamina, the combined mean of left and right putamen voxels was calculated. Significance was determined by using a standard one-tailed *t*-test analysis and Pearson's correlation was used to determine the correlation coefficients.

## Results

### *Voxel-based analysis*

Without the application of brain masks, voxel-based linear regression analysis showed regional decreases in relative anisotropy (RA) in midfrontal white matter regions, the corpus callosum, predominantly in the genu, and the anterior–posterior regions of the corona radiata. The medial cerebral peduncle and bilateral hippocampal complex also showed a significant decline in RA (see Fig. 2 and Table 1).

In contrast, positive correlations with age were found for regions surrounding the external part of the corpus callosum,

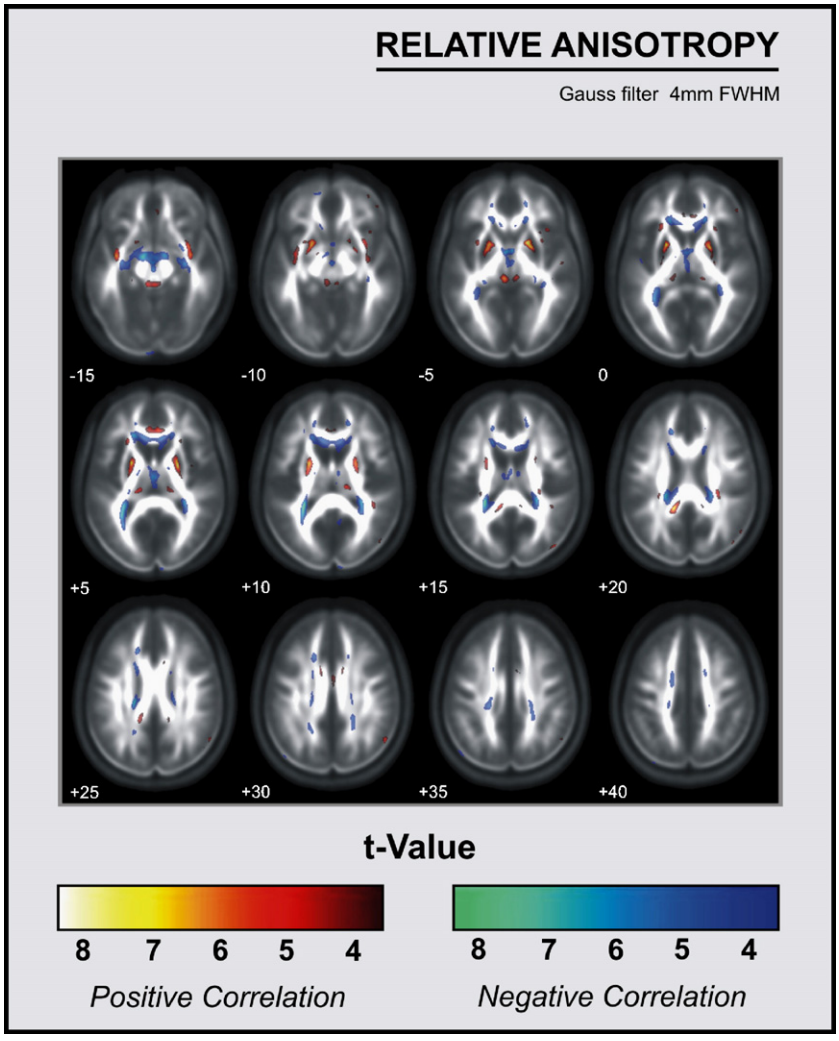


Fig. 2. Normalized and averaged axial RA maps with relative-anisotropy-index-related *t*-score overlays. Figures show positive (red) and negative (blue) correlations.

Table 1
Locations and significance levels ($t$-value of the peak and corrected $p$-value for the cluster) of the main clusters with significant correlation between RA and age

| Relative anisotropy | | MNI coordinates | | | $t$ peak | Cluster $p$ | Masked or unmasked |
|---|---|---|---|---|---|---|---|
| Hemisphere | Structure | $x$ | $y$ | $z$ | | | |
| *Positive correlation* | | | | | | | |
| L | Putamen | −25 | −1 | 6 | 7.58 | <0.0001 | UM |
| R | Putamen | 22 | 2 | 3 | 7.49 | <0.0001 | UM |
| R | Border to genu of corpus callosum | 14 | −46 | 20 | 7.29 | <0.0001 | UM |
| R+L | Border to medial lemniscus | 5 | −29 | −6 | 6.60 | <0.0001 | UM |
| R | Uncinate fasciculus | 38 | −6 | −14 | 6.30 | <0.0001 | UM |
| L | Uncinate fasciculus | −37 | −3 | −16 | 6.07 | <0.0001 | UM |
| L | Posterior thalamus | −14 | −24 | 9 | 5.79 | <0.0001 | UM |
| R+L | Anterior border to splenium of corpus callosum | −4 | 35 | 5 | 5.67 | <0.0001 | UM |
| *Negative correlation* | | | | | | | |
| R | Border to tapetum | 27 | −41 | 12 | 7.90 | <0.0001 | UM |
| R | Internal capsule | 11 | −7 | 13 | 7.22 | <0.0001 | UM |
| L | Border to tapetum | −29 | −38 | 12 | 6.45 | <0.0001 | UM |
| L | Anterior corpus callosum | −18 | 31 | −2 | 6.23 | <0.0001 | UM |
| R | Anterior region of corona radiata | 16 | 30 | 21 | 5.67 | <0.0001 | UM |
| L | Anterior hippocampus | −32 | −14 | −15 | 5.61 | <0.0001 | UM |
| R | Fasciculus occipito-frontalis | 17 | 23 | 27 | 5.38 | <0.0001 | UM |

bilateral inferior fronto-occipital fasciculus and the medial lemniscus. Surprisingly, a statistically significant increase in RA was also seen in putamina bilaterally.

Without the application of brain masks, voxel-based linear regression analysis showed positive significant correlations between the ADC and age in the midfrontal white matter regions and the corpus callosum. Notable increases were observed in periventricular regions, surrounding cerebral peduncle, bilaterally in insular regions, and in the periphery of the brain, mostly focused in frontal and parietal lobes. Regions with significant ADC declines with age were identified in the internal capsule bilaterally, surrounding the exterior part of corpus callosum and in the pontine cistern (see Fig. 3 (top) and Table 2).

With brain masking, linear regression analysis found significant correlations in the same regions (see Fig. 3 (bottom) and Table 2). However, the sign of the correlation of ADC values with age was reversed in insular regions (bilateral), right inferior frontal plane, and in the periventricular area. In other regions where the ADC was correlated with age, the sign of the correlation coefficients was kept constant when brain masking was applied. Examples are the negative correlation in the genu and the posterior limb of the internal capsule as well as the pontine cistern. Positive correlations in both masked and unmasked ADC maps were found in the genu of the corpus callosum.

When the pattern of the brain mask S.D. maps was compared with the spatial distribution of voxels, for which the sign of the ADC-versus-age correlation changes with brain masking, we observed that most of the sign-changing regions shared high S.D. (see Fig. 4a). In detail, 89.5% of the respective voxels (with $t>3.0$) exhibited S.D. values higher than 0.1. This might be interpreted by brain/non-brain variances in these areas causing highly age-correlated effects as the underlying brain atrophy is correlated with age. Since an increase of CSF with age is expected, correlations must be negative if the ADC values in the CSF are set to zero when brain masking is performed and they must be positive otherwise. Consequently, sign changes of the ADC-versus-age correlation coefficients were introduced in the assessment of the observed regional correlations to be caused by morphological changes or to represent actual diffusion parameter changes (see Table 2).

### *Region-of-interest analysis*

#### *Corpus callosum*

A significant negative correlation between RA and age was obtained in the anterior part of the corpus callosum, indicating a linear decrease of RA with age ($r=-0.4$, $p<0.002$). There was no significant correlation between age and ADC ($r=0.15$) in this region, although a positive tendency was observed. Nor were there significant effects on ADC ($r=-0.08$) or RA ($r=-0.2$) in the posterior corpus callosum (see Fig. 5).

#### *Putamen*

RA showed a significant increase in the putamina with age ($r=0.58$, $p<0.001$; see Fig. 6a), both in each putamen and in the total mean value. No significant correlation was obtained in the putamina between age and ADC ($r=-0.018$) (see Fig. 6b).

## Discussion

Voxel-based analysis of tissue water diffusion–akin to voxel-based morphometry–is a fully automated whole brain imaging data processing technique allowing for the identification of specific local differences in brain tissue properties on a voxel-by-voxel basis. In the present study, several brain areas were associated with aging on the base of tissue-water diffusion data, not only regionally as previously shown by studies focusing on ROI-based analysis, but also with voxel-size resolution. The voxel-based approach for the statistical analysis of diffusion parameter data allows whole-brain searches for significant effects without any need for a priori regionally selective hypotheses. However, our results show that the interpretation of each significant region has to be undertaken very carefully because the voxel-based statistical analysis in diffusivity studies may yield a mixture of different effects, particularly in the presence of atrophy.

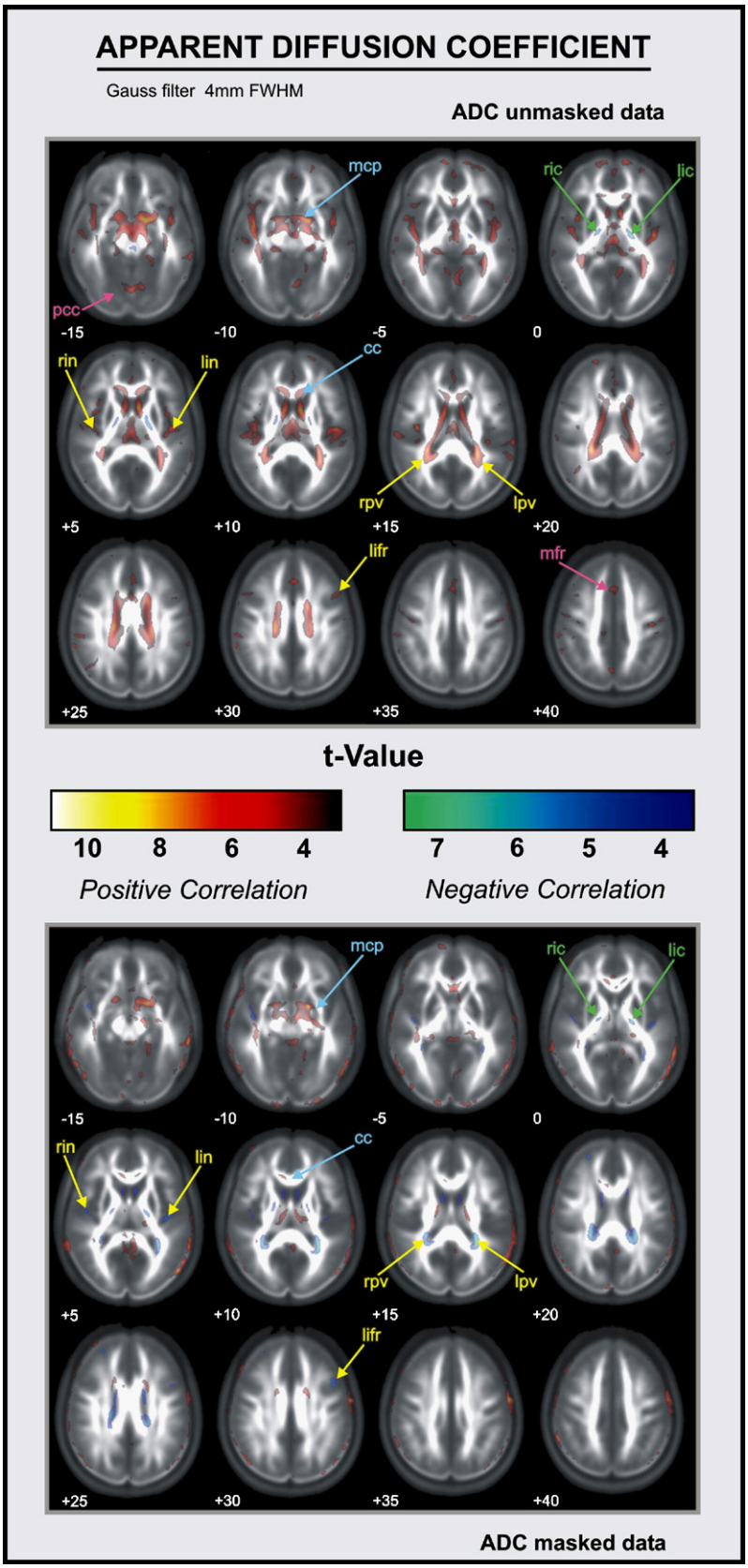
APPARENT DIFFUSION COEFFICIENT
Gauss filter 4mm FWHM
ADC unmasked data
mcp
ric
lic
pcc
-15
-10
-5
0
rin
lin
cc
rpv
lpv
+5
+10
+15
+20
lifr
mfr
+25
+30
+35
+40
t-Value
10 8 6 4
Positive Correlation
7 6 5 4
Negative Correlation
mcp
ric
lic
-15
-10
-5
0
rin
lin
cc
rpv
lpv
+5
+10
+15
+20
lifr
+25
+30
+35
+40
ADC masked data

Table 2
Locations and significance levels (*t*-value of the peak and corrected *p*-value for the cluster) of the main clusters with significant correlation between ADC and age

| Apparent diffusion coefficient | | MNI coordinates | | | *t* peak | Cluster *p* | Masked or unmasked |
|---|---|---|---|---|---|---|---|
| Hemisphere | Structure | *x* | *y* | *z* | | | |
| *Positive correlation for unmasked data and negative for masked data* | | | | | | | |
| R | Insula/Sylvian fissure | 49 | −16 | 8 | 8.87 | <0.0001 | UM |
| | | 39 | −19 | 2 | 5.30 | <0.0001 | M |
| R | Border to lateral ventricle | 8 | 7 | 8 | 8.18 | <0.0001 | UM |
| | | 6 | 11 | 2 | 5.30 | <0.001 | M |
| L | Border to lateral ventricle | −10 | 5 | 12 | 7.44 | <0.0001 | UM |
| | | −15 | 6 | 23 | 4.95 | <0.001 | M |
| L | Border to splenium of corpus callosum | −21 | −22 | 27 | 7.92 | <0.0001 | UM |
| | | −26 | −36 | 20 | 6.05 | <0.0001 | M |
| L | Insula/Sylvian fissure | −41 | −14 | 14 | 7.47 | <0.0001 | UM |
| | | −43 | −11 | −8 | 5.07 | <0.001 | M |
| R | Inferior frontal region | 44 | −17 | 48 | 7.28 | <0.0001 | UM |
| | | 45 | −16 | 50 | 6.08 | <0.002 | M |
| *Positive correlation only for unmasked data* | | | | | | | |
| L | Posterior cerebellar cistern, surrounding tent cerebellum | −9 | −81 | −22 | 6.32 | <0.0001 | UM |
| R+L | Midfrontal regions | −1 | 22 | 38 | 6.16 | <0.0001 | UM |
| *Negative correlation for masked and unmasked data* | | | | | | | |
| R | Internal capsule | 19 | −14 | −1 | 6.78 | <0.0001 | UM |
| | | 19 | −14 | 0 | 6.32 | <0.002 | M |
| L | Internal capsule | −19 | −10 | 0 | 5.44 | <0.005 | UM |
| | | −19 | −10 | 1 | 4.86 | <0.03 | M |
| *Positive correlation for masked and unmasked data* | | | | | | | |
| R | Border to middle cerebral peduncle | 16 | 3 | −12 | 9.06 | <0.0001 | UM |
| | | 18 | 4 | −11 | 8.73 | <0.0001 | M |
| R | Anterior corpus callosum | 17 | 5 | 28 | 7.53 | <0.0001 | UM |
| | | 18 | 8 | 27 | 5.94 | <0.0001 | M |

With voxel-wise linear regression analysis several regions showed significant correlations with age, reflecting histological changes accumulated over the lifespan. However, not all of them necessarily mirror real changes inside white matter regions. In periventricular regions, for example, the significant age-related changes in both ADC and RA values may well be due to the ventricular enlargement that occurs with aging. The impossibility of fitting all the ventricles perfectly by the normalization procedure suggests that, even after normalization, the ventricles of the younger volunteers remain smaller than those of their elder counterparts. If we accept this assumption, an increase in ADC would be due to the comparison of CSF voxels in the older participants with parenchyma in the younger ones, thereby reflecting both an increase in ADC and a decrease in RA values, as our results report. When a particular voxel near the ventricular regions is inspected, it tends to correspond to CSF in the case of the older participants and to parenchyma in the case of the younger ones. This clearly shows that a significant correlation in itself is not sufficient to infer that, in a particular region, age-correlated microstructural changes are prominent. In fact, the CSF–brain interfaces and the outer boundaries of fibre tracts may be susceptible to morphologic involvement. Therefore, a further assessment is needed in order to ensure that the pattern observed is not due to morphological alterations arising from problems in the normalization procedure.

Although these findings seem to indicate morphological origins, a similar pattern might result from coherence loss in white matter tracts or variations in other histological properties. Specifically, diffusivity and anisotropy may be affected by tissue characteristics such as the average tissue water content, the degree of myelination, the density of neuronal fibres or glial cells (Virta et al., 1999; Beaulieu, 2002). In addition, the partial volume effects of white-matter and non-white-matter components may contribute to the diffusion parameters determined and, consequently, to the results reported in the statistical analysis (Head et al., 2004).

Given that the statistical inference may be affected by a wide range of possible causes, a method is needed in order to discriminate between them, i.e., a tool which can distinguish between micro-structural and global age-related changes. With this aim in mind, a mask procedure was applied to the ADC images in the present study.

Using this mask procedure, inverted correlation patterns were obtained at periventricular borders, bilateral insular regions, the pontine cistern and right inferior frontal plane, indicating that these regions do not exhibit actual white matter changes, but rather

Fig. 3. Normalized and averaged axial RA maps with apparent-diffusion-coefficient-related *t*-score overlays using unmasked data in contrast to masked data. Figures show positive (red) and negative (blue) correlations. The main regions are labelled as posterior cerebellar cistern (pcc), pointine cistern (pc), middle cerebral peduncle (mcp), right internal capsule (ric), left internal capsule (lic), right insula region (rin), left insula region (lin), corpus callosum (cc), right periventricular region (rpv), left periventricular region (lpv), right inferior frontal region (rifr), left inferior frontal region (lifr), middle frontal region (mfr). Arrow colours represent positive correlation for unmasked data and negative for masked data (yellow), positive correlation only for unmasked data (purple), positive correlation for masked and unmasked data (blue), and negative correlation for masked and unmasked data (green).

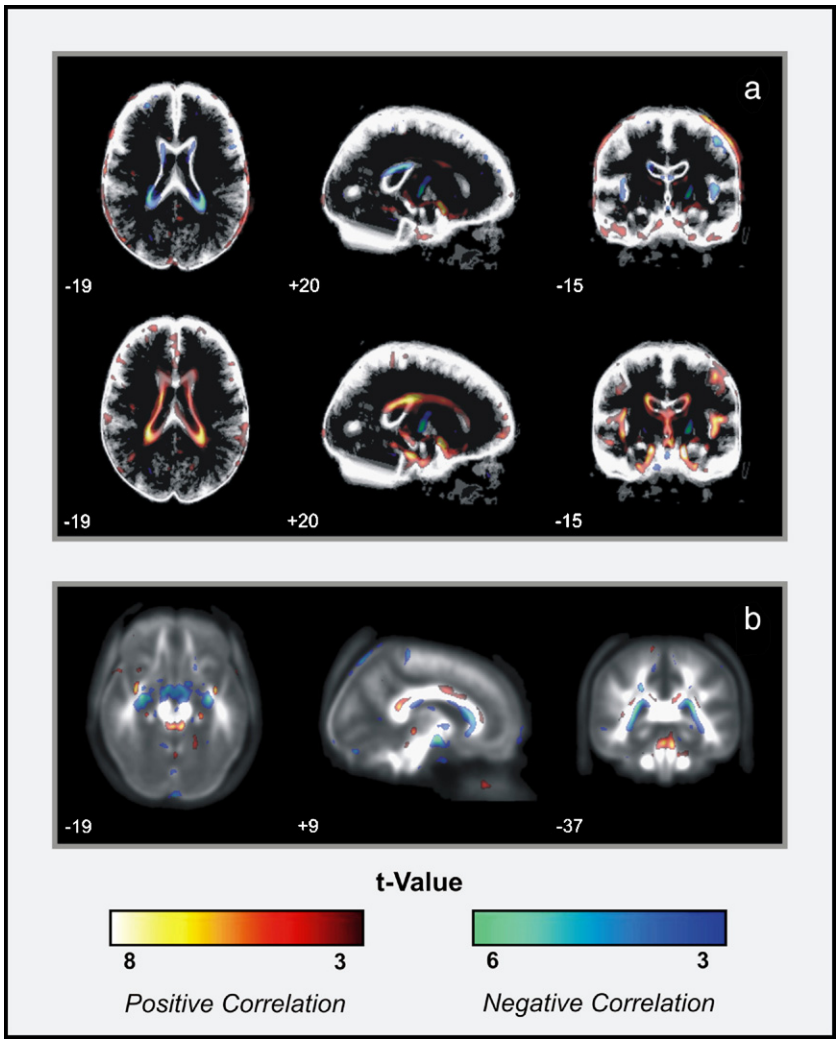


Fig. 4. Inverted patterns obtained using masked (top) versus non-masked (bottom) analysis in ADC maps, overlays on tri-planar standard deviation maps (a). Fibre shifting overlaid in tri-planar RA maps (b). Figures show positive (red) and negative (blue) correlations.

morphological alterations with age. These regions coincided with those reported in a previous morphometric analysis which found age-related macrostructural changes (Good et al., 2001). Interestingly, our candidate regions for predominant morphological influence indicated by the mask procedure are in agreement with the results of Good et al. They reported a positive correlation with age in the Sylvian fissures and a negative correlation in the pontine cistern, corresponding to the sign-inverted correlations that our ADC regression analysis detected when comparing masked and unmasked results (see Figs. 3 and 4a).

Unfortunately, we cannot expect these inverted correlation patterns in the RA images. As masked and non-masked RA values both tend to yield low values in CSF and at CSF–brain interfaces, the masking procedure here is of little use. Nevertheless, if the regions present an inversion of the ADC correlation maps, it is very likely that significant correlations found in RA maps with age in these regions are also involved in morphological alterations and are not due to real white matter changes. In addition, RA might reflect the effects of fibre displacement that has not been properly fitted by the normalization procedure. In this case, the results might be affected by the mixing of fibre tracts with grey matter regions. Indeed, the patterns found in the areas surrounding both the pyramidal tracts and the corpus callosum support this idea. A positive significant correlation of RA with age was observed in the external part of the fibre, suggesting that in the elderly group the pyramidal tracts and the corpus callosum were displaced outwards by the enlargement of the ventricles. Confirmation of this idea was provided by a negative correlation in the internal part of the fibres. The pyramidal tracts and the corpus callosum appear to occupy a more internal location in the youngest subjects. Thus, although in the case of RA images the mask procedure does not allow us to disentangle the influence of normalization, the inverted correlations obtained with age at each side of the fibre tract could provide the key for detecting morphological fibre displacements misaligned in the normalization process (see Fig. 4b).

While for many regions the correlation of ADC and/or RA must be attributed to morphological changes of the brain, there are still several candidate regions for true white-matter changes associated with aging. For example, in agreement with previous reports (Nusbaum et al., 2001; O'Sullivan et al., 2001; Abe et al., 2002; Sullivan and Pfefferbaum, 2003; Salat et al., 2005), our voxel-based analysis revealed significant age-related increases in the ADC in the genu of the corpus callosum, accompanied by a significant decrease in the corresponding RA values. When ROIs

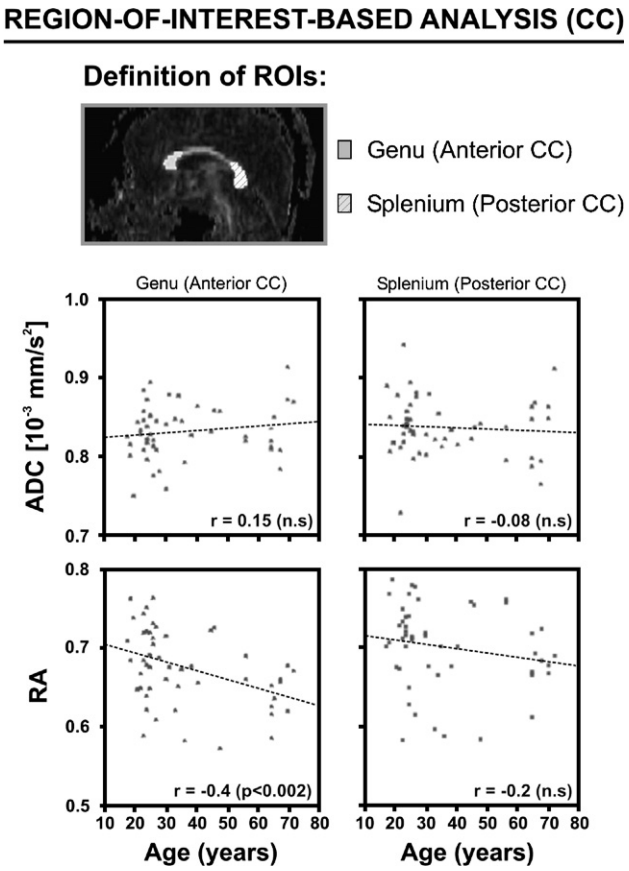


Fig. 5. ROI-based analysis (corpus callosum); scatterplots of both RA-versus-age and ADC-versus-age.

were statistically analysed in native space (without applying a normalization procedure), our results indicated that the anterior fibre tracts are more markedly affected than their posterior counterparts. Recent DTI studies reported very similar results (Head et al., 2004; Salat et al., 2005), associating the decrease in anisotropy with axonal loss, demyelination, increased water content, and combinations of these factors.

Researchers have paid particular attention to both hippocampal and frontal regions and their implications in aging, mostly because of the involvement of these regions in episodic memory and executive functions. Regarding the medial temporal lobe structures, our analysis showed a positive correlation between ADC and age in anterior hippocampal regions, and a negative tendency between RA and age. These results may suggest the presence of real age-related physiological changes in this region. As no inverted patterns were obtained when the masked analysis was performed it is very unlikely that these changes were due only to morphological variations. In fact, volumetric studies tend to report a reduction in the volume of the hippocampus with aging (Good et al., 2001). However, not all studies have observed the same pattern of reduction associated with aging (see for a review, Raz, 2004). These discrepancies may be due to the methodological differences in the definition of the boundaries of the anterior hippocampal regions (Jack et al., 1995; Raz, 2004).

Concerning the frontal regions, a number of histopathological and neuroimaging studies (Kemper, 1994; Resnick et al., 2003; Head et al., 2004; Salat et al., 2005) indicate the vulnerability of frontal white matter in non-demented aging. These results are in agreement with previous pathological reports that have associated this pattern with neuronal loss causing the expansion of the extracellular space (Meier-Ruge et al., 1992), while other studies have described this process as a shrinkage of large neurons (Mrak et al., 1997; Terry et al., 1987). Considering these studies in relation to the present study, our data show that central frontal areas exhibit highly significant positive correlations between age and ADC values. Moreover, this effect converges with the significant negative correlation obtained between age and RA in the same region. These results are also in agreement with previous findings (Head et al., 2004; Salat et al., 2005). Therefore, it is very likely that this pattern of correlations is due to actual white-matter changes. The lack of an inverted pattern of correlations when the mask analysis was applied further supports this idea.

However, a word of caution is in order, because frontal areas may also be prone to increased partial volume effects due to their susceptibility to macrostructural volume loss with age (Raz, 2000); this would have a negative effect on the mask analysis. Furthermore, the high variability in sulcal boundaries between subjects makes it difficult to obtain a perfect fit at the microstructural level. In principle, we cannot rule out the

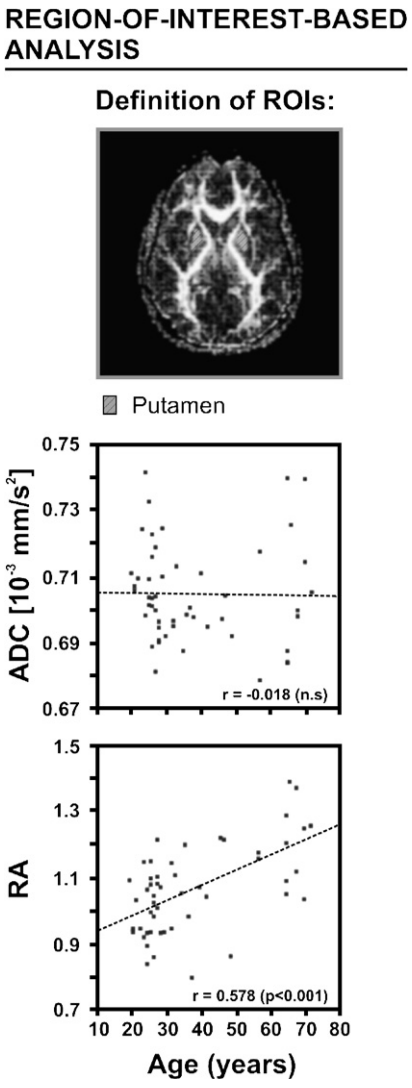


Fig. 6. ROI-based analysis (putamina); scatterplots of both RA-versus-age and ADC-versus-age.

possibility that actual white-matter changes and morphological variations interact in the pattern of results observed.

In agreement with the significant age-related decline of the fractional anisotropy in the internal capsule reported by Virta et al. (1999), and Salat et al. (2004), our results replicated this negative correlation between anisotropy and aging. In addition, in the same region a significant negative correlation in ADC was found in both the masked and the unmasked analysis. It is difficult to determine the biological significance of this negative correlation between ADC and age, as in other parts of the brain the correlations observed between these two variables (which must be attributed to microstructural changes) tend to be positive. However, our results suggest that actual white matter age-related changes in the internal capsule are responsible for this pattern of correlation.

Finally, we were surprised to find a highly significant increase of the RA values in the putamen. This result is consistent with a recent study of ADC and RA age-related changes in several brain regions (Bhagat and Beaulieu, 2004), in which the putamen was the only structure that showed a certain increase in anisotropy with age. However, the authors did not propose any pathophysiological explanation for this result. Additionally, in the entire lentiform nucleus, Abe et al. (2002) observed a slight increase in diffusion anisotropy with age ($p=0.094$). To the best of our knowledge, these are the only reports that provide explicit observations of ROI-based measurements of anisotropy in subcortical grey matter regions and its relationship with aging. Previous structural MRI studies revealed a reduction in the volume of the putamen with increasing age (Good et al., 2001; Raz, 2004). A very early pathological report (Bugiani et al., 1978) found a significant negative correlation between age and cell count in the putamen. In a recent morphometric study, Brickman et al. (2003) reported a partial pervasion of the putamen by axonal projections. As a hypothetical explanation for the positive correlation observed between RA in the putamen and age, it appears that age-related cell loss might affect isotropic cell structures to a higher degree than pervasive axons leaving a raised partial volume of larger anisotropy. However, this is only speculation and a microphysiological explanation is required.

Thus far, we have emphasized the utility of voxel-based diffusion parameter analysis, in contrast to the ROI analysis. However, the role of smoothing data in terms of spatial resolution requires further discussion. Image volume data are frequently smoothed in statistical MRI data analysis so that they can be approximated to a Gaussian random field, which enhances the sensitivity of the statistical analysis and reduces the inter-subject variance. This latter effect is particularly helpful when a non-optimized normalization process occurs, since the image blurring that is obtained reduces the inter-subject differences. The benefits to be derived from Gaussian kernel filtering on the voxel-based diffusivity data have been discussed by Jones et al. (2005). However, if we adhere to the matched filter theorem, smoothing severely diminishes the resolution of diffusion analysis. Thus, because of the robust statistical effect encountered in our study the data were smoothed with a small Gaussian filter of 4 mm FWHM, which enabled us to analyse the present data at a microstructurally meaningful level. However, further studies are needed to determine an optimal smoothing kernel value. Additionally, it is important to bear in mind that some regions, even after applying moderate levels of smoothing, might exhibit non-normally distributed residuals and consequently, statistical parametric tests might not be the most adequate ones (Jones et al., 2005). Non-parametric analyses might be required in order to examine this issue more appropriately.

## Conclusions

As noted above, the normalization process has certain limitations when conducting a voxel-based analysis. Given these limitations, great care must be exercised both in obtaining and in interpreting DTI data, in particular when analysing white matter changes and the effects of aging, where different underlying processes may co-occur. Anatomically defined regions-of-interest may be used to corroborate results from voxel-based analysis, allowing white matter to be tested without the influence of the normalization process (Salat et al., 2005).

Furthermore, linear regression analysis may not be the only statistical approach for investigating white matter changes. Non-linear effects over age may also influence the results observed; if so, non-linear methods are needed to delineate the time course.

Despite these disparities in the possible interpretations given to the DTI analysis, it is clear that DTI is still a highly sensitive method for the evaluation of the underlying microstructure of the fibre tracts. Therefore, as long as researchers are aware of possible artifacts arising from these methodological constraints, voxel-based analysis is a very useful approach for identifying and comparing age-related microstructural white matter alterations in the whole brain. However, additional tools, such as the masking procedure described here, are needed in order to validate these results. In this direction, Smith et al. (2006) have recently proposed a straightforward method to appropriately match previously skeletonised fibre structures and to carry out statistics only for those voxels that remain within the fibre skeletons. This method can be expected to be very important in future studies in order to compare white matter fibre tract changes across subjects but it would not detect systematic changes of diffusion properties in regions like the putamen.

Finally, it is necessary to point out that although the proposed method attempts to disentangle actual changes in diffusivity from changes that are due to underlying morphological age-dependent differences, it does not reveal how age-related diffusivity changes can be affected by other tissue characteristics such as differences in average tissue water content, the degree of myelination and the density of neuronal fibres or glial cells.

## Acknowledgments

We would like to thank our colleagues Ruth de Diego, Toni Cunillera and Anna Mestres for helpful comments on earlier drafts of this paper. This study was supported by an MCYT Grant (BSO2002-01211 to ARF), a pre-doctoral grant from the University of Barcelona (Programa Propi UB to EC), a grant from the Deutsche Forschungsgemeinschaft (SFB 426, TP D1,D4) and the Center of Advanced Imaging Magdeburg (CAI, BMBF grant 01GO0504).

## References

Abe, O., Aoki, S., Hayashi, N., Yamada, H., Kunimatsu, A., Mori, H., Yoshikawa, T., Okubo, T., Ohtomo, K., 2002. Normal aging in the central nervous system: quantitative MR diffusion-tensor analysis. Neurobiol. Aging 23, 433–441.

Ashburner, J., Friston, K.J., 1999. Nonlinear spatial normalization using basis functions. Hum. Brain Mapp. 7, 254–266.

Ashburner, J., Friston, K.J., 2001. Why voxel-based morphometry should be used. NeuroImage 14, 1238–1243.

Beaulieu, C., 2002. The basis of anisotropic water diffusion in the nervous system—a technical review. NMR Biomed. 15, 435–455.

Bhagat, Y.A., Beaulieu, C., 2004. Diffusion anisotropy in subcortical white matter and cortical gray matter: changes with aging and the role of CSF-suppression. J. Magn. Reson. Imaging 20, 216–227.

Bodammer, N., Kaufmann, J., Kanowski, M., Tempelmann, C., 2004. Eddy current correction in diffusion-weighted imaging using pairs of images acquired with opposite diffusion gradient polarity. Magn. Reson. Med. 51, 188–193.

Brickman, A.M., Buchsbaum, M.S., Shihabuddin, L., Hazlett, E.A., Borod, J.C., Mohs, R.C., 2003. Striatal size, glucose metabolic rate, and verbal learning in normal aging. Brain Res. Cogn. Brain Res. 17, 106–116.

Bugiani, O., Salvarani, S., Perdelli, F., Mancardi, G.L., Leonardi, A., 1978. Nerve cell loss with aging in the putamen. Eur. Neurol. 17, 286–291.

Chen, Z.G., Li, T.Q., Hindmarsh, T., 2001. Diffusion tensor trace mapping in normal adult brain using single-shot EPI technique. A methodological study of the aging brain. Acta Radiol. 42, 447–458.

Chun, T., Filippi, C.G., Zimmerman, R.D., Ulug, A.M., 2000. Diffusion changes in the aging human brain. Am. J. Neuroradiol. 21, 1078–1083.

Gideon, P., Thomsen, C., Henriksen, O., 1994. Increased self-diffusion of brain water in normal aging. J. Magn. Reson. Imaging 4, 185–188.

Good, C.D., Johnsrude, I.S., Ashburner, J., Henson, R.N., Friston, K.J., Frackowiak, R.S., 2001. A voxel-based morphometric study of ageing in 465 normal adult human brains. NeuroImage 14, 21–36.

Head, D., Buckner, R.L., Shimony, J.S., Williams, L.E., Akbudak, E., Conturo, T.E., McAvoy, M., Morris, J.C., Snyder, A.Z., 2004. Differential vulnerability of anterior white matter in nondemented aging with minimal acceleration in dementia of the Alzheimer type: evidence from diffusion tensor imaging. Cereb. Cortex 14, 410–423.

Jack Jr., C.R., Theodore, W.H., Cook, M., McCarthy, G., 1995. MRI-based hippocampal volumetrics: data acquisition, normal ranges, and optimal protocol. Magn. Reson. Imaging 13, 1057–1064.

Jones, D.K., Symms, M.R., Cercignani, M., Howard, R.J., 2005. The effect of filter size on VBM analyses of DT-MRI data. NeuroImage 26, 546–554.

Kemper, T.L., 1994. Neuroanatomical and neuropathological changes during aging and dementia. In: Albert, M.L., Knoefel, J.E. (Eds.), Clinical Neurology of Aging. Oxford Univ. Press, New York, pp. 3–67.

Kubicki, M., Westin, C.F., Maier, S.E., Mamata, H., Frumin, M., Ersner-Hershfield, H., Kikinis, R., Jolesz, F.A., McCarley, R., Shenton, M.E., 2002. Diffusion tensor imaging and its application to neuropsychiatric disorders. Harv. Rev. Psychiatry 10, 324–336.

Marner, L., Nyengaard, J.R., Tang, Y., Pakkenberg, B., 2003. Marked loss of myelinated nerve fibers in the human brain with age. J. Comp. Neurol. 462, 144–152.

Meier-Ruge, W., Ulrich, J., Bruhlmann, M., Meier, E., 1992. Age-related white matter atrophy in the human brain. Ann. N. Y. Acad. Sci. 673, 260–269.

Moseley, M., 2002. Diffusion tensor imaging and aging—A review. NMR Biomed. 15, 553–560.

Mrak, R.E., Griffin, S.T., Graham, D.I., 1997. Aging-associated changes in human brain. Review. J. Neuropathol. Exp. Neurol. 56 (12), 1269–1275.

Nusbaum, A.O., Tang, C.Y., Buchsbaum, M.S., Wei, T.C., Atlas, S.W., 2001. Regional and global changes in cerebral diffusion with normal aging. Am. J. Neuroradiol. 22, 136–142.

O'Sullivan, M., Jones, D.K., Summers, P.E., Morris, R.G., Williams, S. C., Markus, H.S., 2001. Evidence for cortical "disconnection" as a mechanism of age-related cognitive decline. Neurology 57, 632–638.

Papadakis, N.G., Xing, D., Huang, C.L., Hall, L.D., Carpenter, T.A., 1999. A comparative study of acquisition schemes for diffusion tensor imaging using MRI. J. Magn. Reson. 137, 67–82.

Pfefferbaum, A., Sullivan, E.V., 2003. Increased brain white matter diffusivity in normal adult aging: relationship to anisotropy and partial voluming. Magn. Reson. Med. 49, 953–961.

Pierpaoli, C., Basser, P.J., 1996. Toward a quantitative assessment of diffusion anisotropy. Magn. Reson. Med. 36, 893–906.

Raz, N., 2000. Aging of the brain and its impact on cognitive performance: integration of structural and functional findings. In: Craik, F.I.M., Salthouse, T.A. (Eds.), Handbook of Aging and Cognition, vol. 2. Erlbaum, Mahwah, NJ, pp. 1–90.

Raz, N., 2004. The aging brain observed in vivo: differential changes and their modifiers. In: Cabeza, R., Nyberg, L., Park, D. (Eds.), Cognitive Neuroscience of Aging. Linking Cognitive and Cerebral Aging. Oxford Univ. Press, New York, pp. 19–57.

Resnick, S.M., Pham, D.L., Kraut, M.A., Zonderman, A.B., Davatzikos, C., 2003. Longitudinal magnetic resonance imaging studies of older adults: a shrinking brain. J. Neurosci. 23, 3295–3301.

Salat, D.H., Tuch, D.S., Greve, D.N., van der Kouwe, A.J., Hevelone, N. D., Zaleta, A.K., Rosen, B.R., Fischl, B., Corkin, S., Rosas, H.D., Dale, A.M., 2005. Age-related alterations in white matter microstructure measured by diffusion tensor imaging. Neurobiol. Aging 26, 1215–1227.

Skare, S., Hedehus, M., Moseley, M.E., Li, T.Q., 2000. Condition number as a measure of noise performance of diffusion tensor data acquisition schemes with MRI. J. Magn. Reson. 147, 340–352.

Smith, S.M., Jenkinson, M., Johansen-Berg, H., Rueckert, D., Nichols, T. E., Mackay, C.E., Watkins, K.E., Ciccarelli, O., Cader, M.Z., Matthews, P.M., Behrens, T.EJ., 2006. Tract-based spatial statistics: voxelwise analysis of multi-subject diffusion data. NeuroImage 31, 1487–1505.

Sullivan, E.V., Pfefferbaum, A., 2003. Diffusion tensor imaging in normal aging and neuropsychiatric disorders. Eur. J. Radiol. 45, 244–255.

Terry, R.D., Deteresa, R., Hansen, L.A., 1987. Neocortical cell counts in normal human adult aging. Ann. Neurol. 21, 530–539.

Tovar-Moll, F., Moll, J., de Oliveira-Souza, R., Bramati, I., Andreiuolo, P.A., Lent, R., 2006. Neuroplasticity in human callosal dysgenesis: a diffusion tensor imaging study. Cereb. Cortex (Apr, Electronic publication ahead of print).

Virta, A., Barnett, A., Pierpaoli, C., 1999. Visualizing and characterizing white matter fiber structure and architecture in the human pyramidal tract using diffusion tensor MRI. Magn. Reson. Imaging 17, 1121–1133.

Wakana, S., Jiang, H., Nagae-Poetscher, L.M., van Zijl, P.C., Mori, S., 2004. Fiber tract-based atlas of human white matter anatomy. Radiology 230, 77–87.

Woods, R.P., Grafton, S.T., Holmes, C.J., Cherry, S.R., Mazziotta, J.C., 1998. Automated image registration: I. General methods and intrasubject, intramodality validation. J. Comput. Assist. Tomogr. 22, 139–152.